International Journal of GEOMATE, Oct., 2017, Vol.13, Issue 38, pp.178-185
Geotec., Const. Mat. & Env., ISSN:2186-2990, Japan, DOI: https://doi.org/10.21660/2017.38.77026

STRENGTH CHARACTERISTICS OF COMPACTED SOIL WITH PARTICULAR REFERENCE TO SOIL STRUCTURE AND ANISOTROPY

*Shunzo Kawajiri[1], Takayuki Kawaguchi[1], Shintaro Yamasaki[1], Dai Nakamura[1], Satoshi Yamashita[1] and Satoru Shibuya[2]

[1] Dept. of Civil and Environmental Engineering, Kitami Institute of Technology, Japan;
[2]Graduate school of Engineering, Kobe University, Japan

*Corresponding Author, Received: 11 April 2017, Revised: 24 April 2017, Accepted: 24 May 2017

ABSTRACT: In this paper, the effects of compaction method on deformation and strength properties of a sandy soil were examined by means of triaxial and unconfined compression tests and bender element test. A X-ray CT scan was also employed for providing us with image of structure of two sandy soils (n.b., sample A and B). The undrained shear strength and dilatancy characteristics were seemingly affected by the compaction method employed, and also the aspect depended on the soil type. The G_{hh}/G_{vh} -value of sample A was larger than that of sample B. The result would mean that the G_{hh}/G_{vh} -value reflecting soil anisotropy is strongly related to the shear strength and dilatancy characteristics. In addition, the variation of ρ_d and D_c of the statically compacted specimens is more significant than that of the dynamically compacted specimens. These variations in terms of ρ_d and D_c may also affect the deformation and strength characteristics.

Keywords: Compacted Soil, Strength Characteristic, Soil Structure, Anisotropy

1. INTRODUCTION

Filling structures such as road embankments, levee and residential land are built by compacting geomaterials with designated methods. Therefore, research results of mechanical characteristics of compacted geomaterials by laboratory soil property tests have been reported for many years. Focusing on compaction methods for preparing specimens of laboratory soil property tests (i.e. mechanical tests), compaction with dynamic methods such as impact or vibration, or static methods with uniform pressure without impact, vibration, or the like were studied. These methods can be translated to vibration roller (dynamic) and road roller (static) respectively in the field. According to past research on the mechanical characteristics of soil properties with laboratory tests, strength of specimens depends on the compaction method employed. Especially, difference in strength is often attributed to difference in soil structure. Regarding research results of samples containing fine fraction, Yong and Warkentin[1] reported that clay samples with shear applied in the compaction direction, which is perpendicular to the layer surface, show larger strength when compacted statically rather than dynamically, and those with shear applied perpendicular to compaction direction, which is parallel to the compaction layer, show the opposite trend, because statically compacted samples have oriented structure whereas dynamically compacted samples have random structure. Seed et al. [2] and Onitsuka et al. [3] reported similar results, where Seed et al. used a triaxial undrained shear test with silty clay more wet than optimum water content, and Onitsuka et al. used a box shear test with white clay. Yokohama et al. [4] reported that degree of compaction and water content affect strength characteristics and permeability, because horizontal and vertical array of coarse and fine fraction depend on degree of compaction and water content from experimental results using silty sand with low plasticity. Meanwhile, the relationship between anisotropy and characteristics of strength of soil structure of classified sandy soil with comparatively uniform grain size was reported by Oda[5], and Arthur and Menzies[6]. Especially, Oda examined details of large variance in deformation and strength characteristics, which is caused by the angle δ between the direction of maximum principal stress σ_1 and the deposition surface, by observing structural anisotropy of a particle array formed during deposition with a microscope for sandy soil.

The static method for preparing specimens in the above-mentioned studies is usually compaction with a loading device using, for example, hydraulic pressure with a full cross section piston having the same diameter as the mold for specimen preparation. The dynamic method for preparing specimens is either prodding samples by a metal prodding bar or rammer having a smaller diameter than the mold for specimen preparation, or putting a vibrator to the side surface of the mold for specimen preparation for compaction. However, only a few papers have reported on mechanical characteristics of specimens prepared by a full cross section piston for dynamic compaction, and therefore, knowledge on the mechanical characteristics of such specimens is very limited.

In this research, specimens were prepared using different compaction methods from two types of geomaterials with slightly different soil properties, in order to examine basic mechanical characteristics with consolidated undrained and drained triaxial compression tests and unconfined compression test, and then a bender element (BE hereinafter) test was carried out to measure anisotropy of elasticity coefficient, which should reflect orientation of soil structure, for examining difference in deformation and strength characteristics in terms of soil structure. X-ray CT scan and observations of cross-sectional images were carried out to understand internal structures of specimens, and to explain triaxial and unconfined compression test, as well as BE test results.

2. TESTING PROCEDURES

2.1 Test materials and specimens

Two kinds of fine-gravelly-sand used for expanding levees were used as samples in this study. Maximum grain size had been adjusted to D_{max} = 19 mm considering specimen size for laboratory tests. Sample A had soil particle density, ρ_s = 2.67 g/cm^3, liquid limit, w_L = 34%, and plastic limit, w_P = 21%, while those of sample B were ρ_s = 2.65 g/cm^3, w_L = 31%, and w_P = 19%. Fig. 1 shows grain size distribution of these samples. It can be

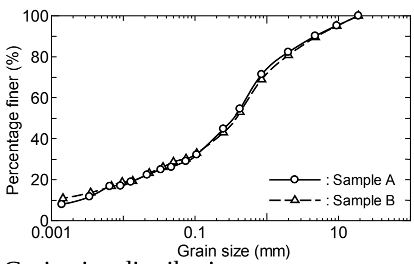

Fig.1 Grain size distribution

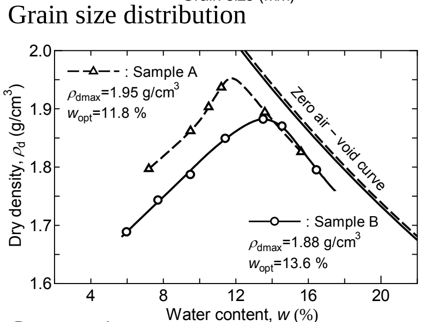

Fig.2 Compaction curves

seen in this figure that samples A and B have almost equal texture of graining, with sample B having slightly higher clay fraction and lower sand matter. Fig. 2 shows compaction curve of these samples obtained in accordance with the A-a method stipulated by JIS A 1210(Compaction energy, E_c = 550kJ/m^3(Standard proctor)). As shown in this figure, samples A and B had different properties to a certain degree; sample B had larger optimum water content, w_{opt} than sample A while maximum dry density, ρ_{dmax} turned out to be lower compared with that of sample A.

Shapes of the specimens used in this research were columnar with a diameter of 10 cm and a height of 20 cm (hereinafter called "Cylinder specimen"), and a regular hexahedron with one side 12 cm (hereinafter called "Cube specimen"). In each specimen, each compacted layer had a thickness of 4 cm, with five layers for cylinder specimens and three layers for cube specimens. Water was added to naturally seasoned samples before thorough agitation to make compiled samples, which were then separated in two parts to prepare specimens with both dynamic and static methods. Photo 1 shows a cylinder specimen prepared by dynamic and static compaction and Photo 2 shows a preparation process of a cube specimen. For dynamic compaction, a compiled sample necessary to obtain designated dry density for one layer was put into the mold, and a piston (plunger) with almost the same cross section was inserted, and then hammered down the handle with a plastic hammer to make each layer the

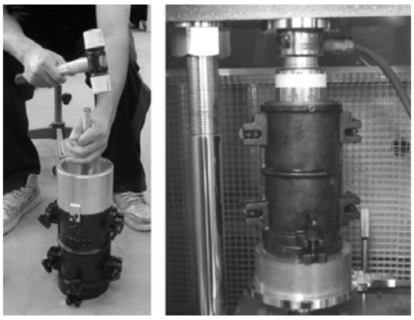

Photo.1 Preparation of cylinder specimen
(Left side: dynamic, Right side: static)

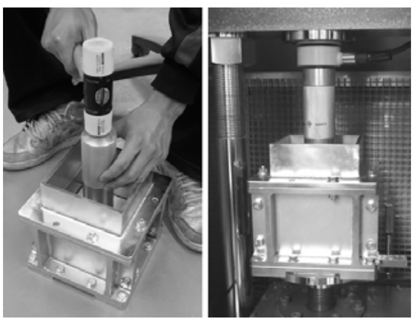

Photo.2 Preparation of cube specimen
(Left side: dynamic, Right side: static)

Table.1 Summary of test condition

<table>
<tr><th rowspan="2">Sample</th><th colspan="2">Triaxial</th><th rowspan="2">Unconfined</th><th rowspan="2">Bender element</th><th rowspan="2">Observation of inner structure</th></tr>
<tr><th>Undarained</th><th>Drained</th></tr>
<tr><td>A</td><td rowspan="2">Cylinder
(ϕ10×20cm)
(p'=50, 100, 150 kPa)
(D_c = 100%, w_{opt})</td><td>—</td><td>—</td><td>Cylinder
(ϕ5×10cm)
(D_c=85, 90, 100%, w_{opt})</td><td>X-ray CT scan
(Cylinder: ϕ5×10cm)
(D_c = 100%, w_{opt})</td></tr>
<tr><td>B</td><td>Cylinder
(ϕ10×20cm)
(p' = 50 kPa)
(D_c = 100%, w_{opt})</td><td>Refer Table. 2</td><td>Cube
(12×12×12cm)
(D_c= 100 %, w_{opt})</td><td>Cross-section observation
(Cube: 12×12 ×12cm)
(D_c = 100%, w_{opt})</td></tr>
</table>

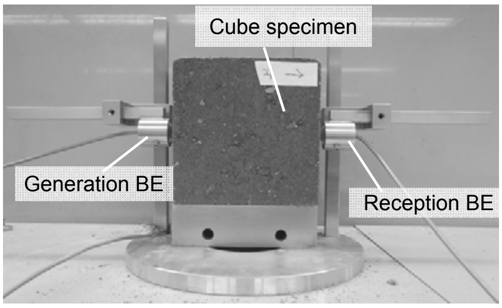

Photo.3 Bender element test for cube specimen

designated height of 4 cm. As for static compaction, after putting the designated amount of compiled specimen in mold just as in dynamic compaction, a loading device was set to touch the load cell, whose piston handle had been firmly joined to the reaction force frame, and then the load table was raised to a designated height manually. The surface was scratched so that layer boundaries would adhere well with each other.

2.1 Test program

Table 1 shows a summary of test conditions. Regarding deformation and strength characteristics, cylinder specimens with diameter of 10 cm and height of 20 cm were used for both samples A and B, which were subjected to a consolidated undrained triaxial compression test. Consolidated drained triaxial compression tests were also carried out with sample B, which was further subjected to an unconfined compression test using the cube specimen to examine the effect on strength anisotropy. These tests all complied with JGS (Japanese Geotechnical Society) test standards. In triaxial tests, the compacted soil specimen was sealed with a rubber membrane in the triaxial apparatus. The sealing conditions were checked by observing air bubbles in a water tank placed between a specimen and a vacuum pump when applying a negative back pressure of around 20kPa. The cell was then filled with de-aired water. The specimen was flushed by supplying distilled water from the bottom of the specimen over a period more than 12 hours. Then, the back pressure was decreased to 90kPa in negative against the cell

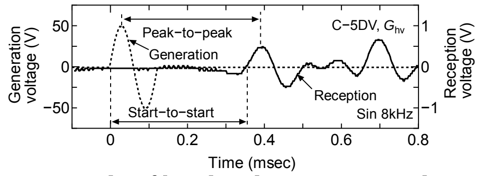

Fig.3 Example of bender element test result

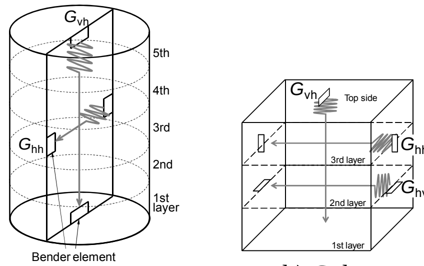

a) Cylinder b) Cube

Fig.4 Types of shear wave

pressure of 70 kPa in negative with which the effective confining pressure was maintained to be the constant value of 20 kPa. The cell pressure, σc and the pore water pressure, *u*w were both raised simultaneously to 220 kPa and 200kPa, and the *B* values for all the specimens were measured by showing the values greater than 0.96. After the sample was saturated, it was isotropically consolidated to the effective consolidation stress, p' equal to 50, 100 and 150 kPa, respectively After the consolidation process, the sample was sheared undrained or drained in compression by using the axial strain rate of $d\varepsilon_a$ / dt = 0.05%/min (Undrained condition), 0.02%/min (Drained condition), up to the axial strain, ε_a of 15 %.

Elastic shear modulus, *G* was also measured by BE test mainly to confirm orientation of soil structure. With sample A, specimens were prepared separately for BE test and mechanical test. For sample B, BE test was carried out with a cube specimen right before the unconfined compression test. Photo 3 shows a sample B subjected to BE test using a tool to enable fixing of BE at a designated position. Because it was extremely difficult to insert BE to this specimen, the tip of the BE was fixed at the specimen surface. Fig. 3 shows one example of BE test results. To calculate *G* from the test results, we basically complied with the method recommended by JGS 0544:2011 "Method for laboratory measurement of shear wave velocity of soils by bender element test" [7].

Fig. 4 shows types of shear wave detected with cylinder and cube specimens, and names of values of G obtained thereby. In this study, G_{hv} was defined as modulus of transverse elasticity obtained for elastic-wave propagating perpendicular to the layer surface, which is perpendicular to the compaction direction, while vibrating horizontally along the layer surface; G_{hh} was defined as that for waves vibrating and propagating horizontally; and G_{vh} that for waves vibrating perpendicularly while propagating horizontally. Incidentally, we interpreted test results assuming that G_{hv} and G_{vh} are identical in accordance with orthotropic elastic theory. Each G value was measured at multiple positions to obtain rigidity distribution within layers and boundaries for some of the specimens.

Sample A was subjected to X-ray CT scan to observe internal structure of the specimen. A specimen with diameter of 5 cm and height of 10 cm was used here to increase accuracy of the scan results. Output data obtained by X-ray CT scan are called GL (Gray Level) values, which are integer values of 16 bit (0 to 65535) for each voxel, and are roughly proportional to average density of material within the voxel [9]. Utilizing this proportionality, the relationship between GL value and ρ_d value was obtained beforehand by measuring specimens with known ρ_d values to determine conversion formula from GL value to ρ_d value. With this conversion formula, height-wise variation of ρ_d and D_c of specimens was observed.

Regarding observation of the cross-section of a sample B specimen, on the other hand, a separately prepared specimen was solidified to prevent soil structure from falling apart and to observe cutting plane with a scanner. The specimen was immersed for several days in paraffin maintained at about 110°C to replace pore air and water with paraffin having a melting point of 70°C, before cooling down to solidify, and then the specimen was cut with a rock cutter [10]. A large amount of air was emitted from the specimen at the onset of immersion in paraffin, but the surface of the specimen remained stable.

3. RESULTS AND DISCUSSION

3.1 Triaxial and unconfined compression test

Fig. 5 shows consolidated undrained triaxial compression test results of samples A and B comparing relation between deviator stress, q and axial strain, ε_a and the relation between excess pore water pressure, Δu and ε_a at undrained shear after consolidation to p' = 100 kPa. For both the dynamic and static specimens, maximum deviator stress q_{max} was larger with sample A than with sample B. q_{max} of static specimen was larger than that of dynamic specimen for all samples, and with specimen A, q_{max} of the static specimen was about two times that of the dynamic specimen. However, q_{max} of the static specimen of sample B was only about 10% larger than that of the dynamic specimen, indicating that the effect of compaction method to deformation and strength characteristics was much smaller as compared with sample A. When focusing on generation behavior of Δu, static and dynamic specimens of sample A showed quite different behavior, where negative Δu was generated with a static specimen having a large q_{max}. On the other hand, such large difference of generation behavior of Δu depending on compaction method was not observed with sample B. Fig. 6 shows consolidated results of drained triaxial compression tests carried out with sample B. Both relationships between q and ε_a, and dilatancy characteristics showed very little dependency on compaction method, and q_{max} showed the opposite trend as compared with undrained triaxial compression test results, where it was somewhat larger with dynamic specimens.

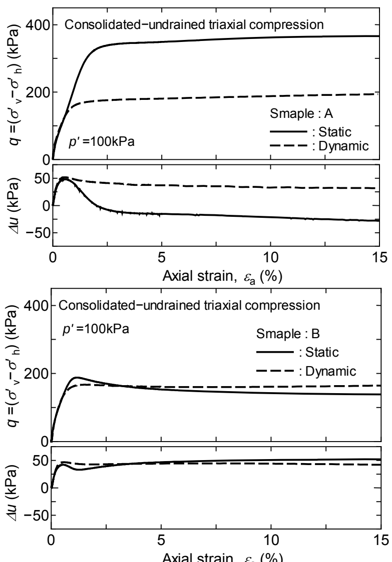

Fig.5 Results of consolidated undrained triaxial compression test (p' = 100kPa)

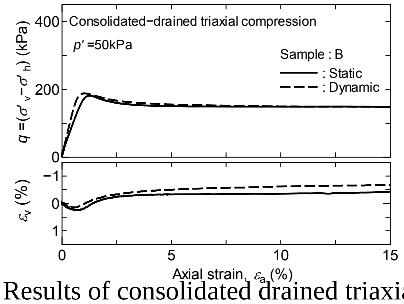

Fig.6 Results of consolidated drained triaxial compression test (p' = 50kPa)

Table.2 Results of unconfined compression test and wet density, dry density, water content of specimens

Specimen	Wet density ρ_t (g/cm^3)	Dry density ρ_d (g/cm^3)	Water content w (%)	Unconfined compression strength, q_u (kPa)	Ratio of q_u (Dynamic/ Static)
Cy-1DV	2.06	1.83	12.6	180	1.15
Cy-1SV	2.05	1.82	12.8	157	
Cy-2DV	2.07	1.84	12.7	191	1.19
Cy-2SV	2.05	1.82	12.7	160	
Cy-3DV	2.07	1.83	12.9	218	1.31
Cy-3SV	2.05	1.82	13.0	167	
Cu-1DV	2.07	1.81	14.0	283	1.39
Cu-1SV	2.06	1.80	14.0	203	
Cu-2DH	2.07	1.82	13.8	189	1.25
Cu-2SH	2.05	1.80	13.9	151	
Cu-3DV	2.05	1.81	12.9	332	1.08
Cu-3SV	2.05	1.82	13.0	308	
Cu-4DH	2.06	1.81	13.8	189	1.24
Cu-4SH	2.05	1.80	13.9	152	
Cu-5DV	2.04	1.81	12.5	339	1.07
Cu-5SV	2.04	1.82	12.6	317	
Cu-6DH	2.03	1.81	12.4	257	1.15
Cu-6SH	2.02	1.80	12.5	223	
Cu-7D	2.07	1.83	13.0	-	-
Cu-7S	2.04	1.81	13.0	-	

Cy: Cylinder specimen, Cu: Cube specimen, D: Dynamic method for compaction, S: Static method for compaction
V: Load direction is vertical to compaction layer, H: Load direction is horizontal to compaction layer

Table 2 is a summary of unconfined compression test results carried out on sample B and physical properties of the specimen. Specimens having the same number as their names were made from the same water content compiled sample; D and S denote dynamic and static compaction; and V and H denote vertically and horizontally loaded to the compaction layer, respectively. Wet density, ρ_t was measured with the specimen immediately before the unconfined compression test, and water content, w was measured with the specimen after the unconfined compression test. As can be seen here, calculated dry density, ρ_d from these results distributed from 1.80 to 1.84 against the target value of 1.83, and w distributed from 12.4 to 14.0 against the target value of 13.2. Fig. 7 shows the relationship between axial stress, σ and axial strain, ε obtained from the unconfined compression test carried out on a cylinder specimen. As can be seen in this figure, the specimen made by dynamic compaction (hereinafter called "Dynamic specimen") had larger unconfined compression strength, which is different from what had been reported in earlier papers [2][3]. In all cases the dry density of specimens shown here is larger with dynamic specimens (see Table-2), but when we compare strength of the cube specimens 3DV and 3SV, and 5DV and 5SV, which are each made from compiled sample with the same water content, the dynamic specimen showed larger strength by about 10% despite the opposite trend of dry density value. Among specimens made from compiled samples with the same water content, dynamic specimens showed larger strength regardless of

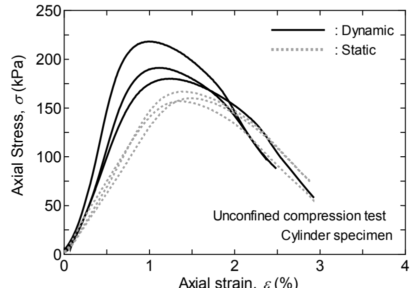

Fig.7 Relationship between q and ε of cylinder specimens

specimen shape or load direction; one interpretation is that even when density and water content are equal, a dynamic specimen has at least 10% larger strength as compared to a specimen made by static compaction (hereinafter called "static specimen"). This means that dynamic specimens may have larger strength with certain samples or shearing methods. Although each specimen is made so as to have equal density (height of specimen), since wet and dry density with most of the static specimens were smaller as compared with the dynamic specimens, samples must have expanded during specimen making and start of the tests. Incidentally, according to results of consolidated undrained triaxial test carried out with saturating specimens made by the same method, compression amount of recompression of static specimens was larger than for dynamic specimens, which further supports this inference. Static specimens showed more dilatancy trend at shearing of consolidated undrained and drained triaxial compression test results as shown in Figures 5 and 6, and undrained shearing strength with static specimens was about 15% larger on average. Conditions of unconfined compression test in this study were rather close to drained and exhausted conditions, since strain rate was comparatively small ($d\varepsilon_a/dt$ = 0.8%/min), and considering that relationship of strength changed with drainage conditions, dilatancy was closely related to the difference in strength between static and dynamic specimens of the samples. However, difference in dilatancy and shear strength at undrained shearing was much smaller than in the control samples, and therefore, the cause of the difference cannot be readily deduced.

Fig. 8 shows comparison of relationship between σ and ε of cubes of 3DV, 3SV, 5DV, 5SV, 6DH, and 6SH, which showed comparatively small w and ρ_d difference. If load direction is the same against layer surface, strength with the dynamic specimen is larger, and, as is widely known, if the preparation method is the same it is more brittle and has larger strength when loaded perpendicular to the layer surface. Onitsuka et al. [3] had shown that strength anisotropy had become opposite with static and dynamic specimens with white clay, but this trend was not seen with sample B.

Fig. 9 shows comparison of unconfined compression strength results obtained with cube specimens. As is widely known, strength tends to be larger when w of specimen is slightly smaller than w_{opt}. It can also be seen here that strength anisotropy of dynamic and static specimens is not much different with this sample; this is different from what had been reported earlier, that static specimens have larger anisotropy because of orientated structure.

The series of triaxial and unconfined compression test results reveal that influence of compaction method to deformation and strength characteristics varies greatly even with samples having similar grain size distributions. Additionally, when compaction method affect deformation and strength characteristics, dilatancy behavior changed depending on compaction method, and considering that relationship of q_{max} value changed with drainage conditions, it could be seen that difference in deformation and strength characteristics depending on compaction method is closely related to dilatancy.

3.2 Bender element test

Fig. 10 shows comparison of BE test results carried out with samples A and B. If G_{hh}/G_{vh}, which is shown as slope of line in the graph, is larger than 1, it is interpreted that the sample has oriented structure, with the degree of orientation increasing with slope [10]. When looking at the difference between samples, G_{hh}/G_{vh} of sample A was 20 to 30% larger than that of sample B. This result was consistent with q_{max} trend of undrained triaxial test results. When focusing on compaction method, G_{hh}/G_{vh} of the static specimen was slightly larger than that of the dynamic specimen with sample A. With sample B, on the other hand, G_{hh}/G_{vh} was almost the same for both compaction methods, which was also consistent with q_{max} trend with triaxial compression test results. Therefore, degree of anisotropy arising from preparation method of specimens is closely related to difference in dilatancy behavior and strength characteristics.

Fig. 11 shows results of BE test carried out with cube specimens of sample B to understand details of height-wise distribution of G. As can be seen in this figure, G of static specimens is generally smaller; dynamic specimens have larger dispersion; and the value tends to be larger for lower layers. Since elastic-waves tend to propagate along the harder part, the above-mentioned difference cannot be directly attributed to strength difference, but it may be possible to infer that the

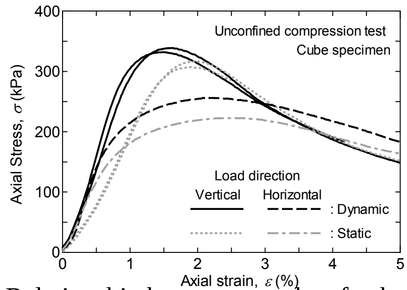

Fig.8 Relationship between q and ε of cube specimens

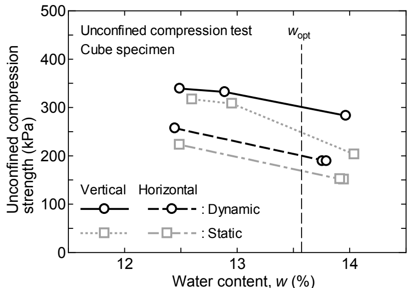

Fig.9 Relationships between unconfined compression and water content

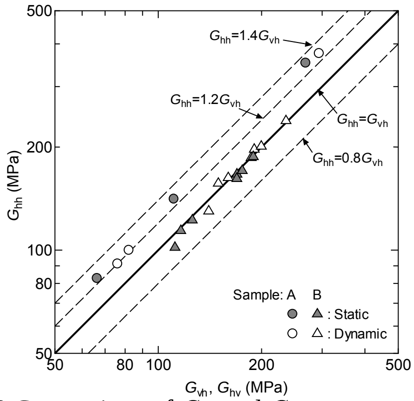

Fig.10 Comparison of G_{vh} and G_{hh}

strength difference is induced by not only dilatancy during shearing, but also rigidity at the initial stage.

3.3 X-ray CT scan and cross-section structure

Fig. 12 shows a comparison of X-ray CT scan images of dynamic and static specimens of sample A. Fig. 13 shows comparison of height-wise distribution of ρ_d and D_c converted from GL values of these specimens. Table 3 further summarizes standard deviation of D_c calculated for a thickness of 20 mm of the 4th, 3rd, 2nd ((1), (2), (3)) layers, and 10 mm of each layer including boundary layers ((4), (5), (6), (7)) to compare details of dispersion of D_c shown in Fig. 13. Standard deviation indicates degree of dispersion of values within a certain range, and as this value becomes larger, so does the dispersion. Standard deviation of each layer ((1), (2), (3)) and cross-section including boundary layers ((4), (5), (6), (7)) show that dispersion is mostly constant except for the lower part of the specimen, and that dynamic specimens have larger standard deviation than the static ones. This shows that height-wise distribution of density of dynamic specimens is less uniform than that of static specimens, which is consistent with the results obtained from Fig. 11.

Fig. 14 shows a comparison of cross-sectional images of dynamic and static specimens of sample B specifically prepared for the observation to examine particle array within the specimen, and illustrations of particles of a specified size extracted from the cross-sectional images. In this figure, each layer is further divided into three sub-layers, and the contour figure of the sum of number of particles with longer side measuring 5 mm or more is also shown. Next to the contour figure is total number of particles. As can be seen from the results, with dynamic specimens, darker areas of the contour figure are situated mostly in the center to the lower part of each layer, and gravel with large grain size seemingly distributes in the center to lower layers. This is also consistent with the results shown in Fig. 11, and may suggest that non-uniformity of height-wise density and rigidity are part of the causes for strength difference.

4. CONCLUSION

In this study, we compacted two types of geomaterials, which were classified as fine-gravelly-sand, by dynamic and static methods using a full cross section piston, which had not been studied much so far, and carried out consolidated undrained and drained triaxial compression tests, unconfined compression tests, BE tests, and observations within specimens, focusing on soil structure and anisotropy in order to investigate differences in deformation and strength characteristics by compaction method and causes of such differences. Obtained results are summarized as follows.

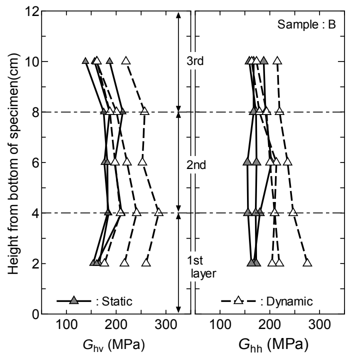

Fig.11 Profile of G for sample B

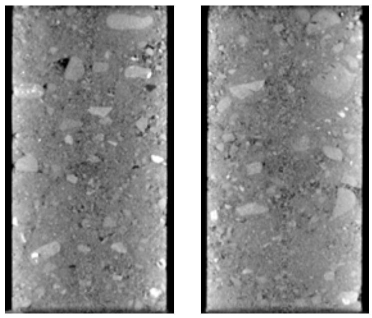

a) Static b) Dynamic

Fig.12 X-ray CT image for sample A

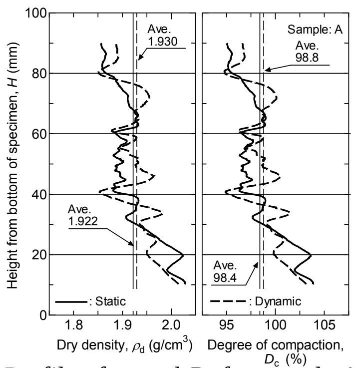

Fig. 13 Profile of ρ_d and D_c for sample A

Table-3 Summarizes of standard deviation of D_c for sample A

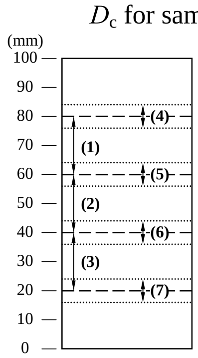

Height from bottom of specimen	Standard deviation of D_c, σ (%)	
	Dynamic	Static
(1) 60 ~ 80	1.42	0.89
(2) 40 ~ 60	1.41	0.38
(3) 20 ~ 40	1.44	1.73
(4) 75 ~ 85	1.44	0.72
(5) 55 ~ 65	0.85	0.82
(6) 35 ~ 45	1.81	1.06
(7) 15 ~ 25	0.52	0.69

1) Difference in strength of static and dynamic specimens can be very large even with samples having similar grain size distribution.
2) Dilatancy seems to be closely related to deformation and strength characteristics difference due to compaction methods.
3) Maximum deviator stress q_{max} obtained from undrained triaxial compression tests and the relationship of values of G_{hh}/G_{vh}, which represents orientation of soil structure, obtained from BE tests were consistent, suggesting that degree of orientation of soil structure affects dilatancy behavior and difference of strength.
4) Dynamic specimens show larger dispersion of height-wise G, and the value becomes larger for lower layers. These results are consistent with X-ray CT scan results and cross-sectional images, suggesting that height-wise density and non-uniformity of rigidity might also be part of the causes for strength dispersion.

Incidentally, load stress at compaction (i.e. pre-compaction pressure) might affect these test results. It is important to obtain pre-compaction pressure by consolidation test at high stress level for quantitative interpretation of the test results, which we could not carry out in this study due to limitations on the performance of test equipment.

5. ACKNOWLEDGEMENTS

We wish to thank Prof. Yoshiaki KIKUCHI (Tokyo University of Science, Former Port and Airport Research Institute) and Dr. Taka-aki MIZUTANI (Port and Airport Research Institute) for advice on X-ray CT scan.

6. REFERENCES

[1] Yong, R. N. and Warkentin, B. P.: Introduction to Soil Behaviour, Macmillan, 1966, pp.106-107.
[2] Seed, H. B., Mitchell, J. K. and Chan, C. K.: Structure and strength characteristics of compacted clays, Journal of SMFD, Proceeding of ACSE, SM5, 1959, pp.87-125.
[3] Onitsuka, K., Hayashi, S., Yoshitake, S., & Oishi, H., Studies on Compression and Strength Anisotropy of Compacted Soils. Soils and foundations, Vol. 19, No. 3, 1979, pp.1467-1471 (in Japanise).
[4] Yokohama, S., Miura, S. and Matsumura, S.: Change in hydromechanical characteristics of embankment material due to compaction state condition, Soils and Foundations, Vol.54, No. 4, 2014, pp.731-747.

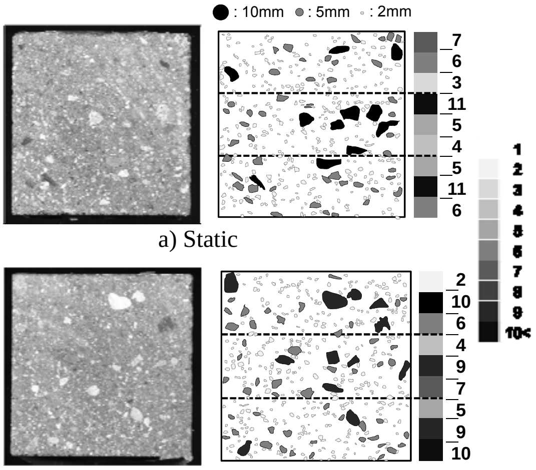

a) Static

b) Dynamic

Fig.14 Cross-sectional images and particle array

[5] Oda, M.: Initial fabrics and their relations to mechanical properties of granular material, Soils and foundations, Vol.12, No.1, 1972, pp.17-36.
[6] Arthur, J.R.F. and Menzies, B.K.: Inherent anisotropy in a sand, Géotechnique, Vol.22, No.1, 1972, pp.115-128.
[7] Japanese Geotechnical Society: JGS 0544:2011, “"Method for laboratory measurement of shear wave velocity of soils by bender element test", 2011.
[8] Kikuchi, Y., Sato, T., Nagatome, T., Mitarai, Y. and Morikawa, Y., Change of Failure Mechanism of Cement Treated Clay by Adding Tire Chips, Geosynthetics in civil and environmental engineering, Part.5 ,2009, pp.374-379.
[9] Yamasaki, S., Chigira, M., A method for making cross-sections of fragile materials from fracture zone and weathering zones by using epoxy resin and paraffin. Journal of Japan Society of Engineering Geology, Vol.50, 2009, pp.289–294
[10] Kawaguchi, T., Yamashita, S., Kawajiri, S., Kataoka, S. and Shibuya, S.: Inherent and induced anisotropy of three natural sedimentary clays reflecting on the elastic shear modulus, Proc. of 4th International symposium on Deformation Characteristics of Geomaterials, IS-Atlanta, Vol.2, 2008, pp.575-578.